Applied Catalysis B: Environmental 188 (2016) 235–244

Contents lists available at ScienceDirect

Applied Catalysis B: Environmental

journal homepage: www.elsevier.com/locate/apcatb

Importance of the oxygen bond strength for catalytic activity in soot oxidation

Jakob M. Christensen[a,*], Jan-Dierk Grunwaldt[a,b], Anker D. Jensen[a]

[a] Department of Chemical and Biochemical Engineering, Technical University of Denmark, Søltofts Plads B229, 2800 Kgs. Lyngby, Denmark
[b] Institute for Chemical Technology and Polymer Chemistry (ITCP), Karlsruhe Institute of Technology, Engesserstrasse 20, 76131 Karlsruhe Germany

ARTICLE INFO

Article history:
Received 8 November 2015
Received in revised form 24 January 2016
Accepted 27 January 2016
Available online 31 January 2016

Keywords:
Soot oxidation
Oxygen bond strength
Heat of chemisorption
Volcano curve
Brønsted-Evans-Polanyi relationship

ABSTRACT

The oxygen bond strength on a catalyst, as measured by the heat of oxygen chemisorption, is observed to be a very important parameter for the activity of the catalyst in soot oxidation. With both intimate contact between soot and catalyst (tight contact) and with the solids stirred loosely together (loose contact) the rate constants for a number of catalytic materials outline a volcano curve when plotted against their heats of oxygen chemisorption. However, the optima of the volcanoes correspond to different heats of chemisorption for the two contact situations. In both cases the activation energies for soot oxidation follow linear Brønsted-Evans-Polanyi relationships with the heat of oxygen chemisorption. Among the tested metal or metal oxide catalysts Co_3O_4 and CeO_2 were nearest to the optimal bond strength in tight contact oxidation, while Cr_2O_3 was nearest to the optimum in loose contact oxidation. The optimum of the volcano curve in loose contact is estimated to occur between the bond strengths of α-Fe_2O_3 and α-Cr_2O_3. Guided by an interpolation principle $Fe_aCr_bO_x$ binary oxides were tested, and the activity of these oxides was observed to pass through an optimum for an $FeCr_2O_x$ binary oxide catalyst, which exhibited a rate constant at 550 °C that was 2.3 times higher than the one for pure α-Cr_2O_3 and 29 times higher than the one for pure α-Fe_2O_3.

1. Introduction

Soot particles in the exhaust from diesel vehicles are likely to cause lung cancer and to affect the climate both locally and globally [1–6]. The soot particles are therefore typically removed from the exhaust gas by filtration through a ceramic filter [7–9]. It is necessary with periodic regeneration of the filter, where the filter temperature is increased, and the soot is oxidized. The growing back pressure due to the soot deposits and the temperature increase required for filter regeneration are associated with increased fuel consumption [10]. To limit the increase in fuel consumption it is desirable to develop soot oxidation catalysts that can lower the regeneration temperature—ideally down to the typical temperature of the exhaust gas [7,11]. Here it is a challenge that the heterogeneously catalyzed soot oxidation is a gas/solid/solid interaction, where the contact between soot and catalyst is very important for the catalytic activity [12–14]. In tests, where soot and catalyst are crushed together (so-called tight contact), the oxidation occurs at a significantly lower temperature, than when soot and catalyst are stirred together (so-called loose contact) [12–14]. TEM studies by Gardini et al [15] on Ag/soot mixtures have indicated that tight contact corresponds to an extensive interface between primary particles of catalyst and soot, whereas loose contact corresponds to fewer contact points at the interface between coagulates of catalyst particles and coagulates of soot particles. In several experiments [11,16–20] with oxidation of soot particles filtered from gas streams by a catalytic filter part of the soot oxidation has been observed to peak at a relatively low temperature in the range characteristic of tight contact with the catalyst, while another part of the soot oxidation has been observed to peak at a higher temperature more characteristic of loose contact with the catalyst. Hence an understanding of both tight and loose contact oxidation may be relevant for real filter applications.

To promote the development of improved catalysts that enable soot oxidation to take place at lower temperatures it is important to identify the parameters that determine the catalytic activity. The surface area of the employed catalyst is known to be of importance [21–23], but an improved understanding of the factors determining the intrinsic activity of a catalytic material would be beneficial. Boreskov et al. [24] proposed that for metal oxide catalysts the oxygen bond strength on the catalyst surface, as measured by the heat of oxygen chemisorption, is a determining factor for activity

* Corresponding author.
E-mail address: jmc@kt.dtu.dk (J.M. Christensen).

http://dx.doi.org/10.1016/j.apcatb.2016.01.068
0926-3373/

in reactions involving oxygen activation. This has been observed to be the case in oxygen activation reactions such as $^{16}O_2/^{18}O_2$ isotopic exchange [24] and oxidation of CH_4 [24], C_3H_6 [25], H_2 [24–27] and CO [28–30]. The activity in the catalytic oxidation of CO on thin metal oxide films has also been correlated to the activation energy for oxygen desorption [31], which scales with the heat of chemisorption. Furthermore, the heat of chemisorption has also been found to be among the factors that play a role for the selectivity in oxidation of benzaldehyde [32] and methanol [33]. It is therefore relevant to investigate, if the heat of oxygen chemisorption can explain the trends in catalytic activity for soot oxidation, and that is the topic of the present work.

2. Materials and methods

2.1. Catalysts used for screening experiments

The catalysts used in the screening studies were bulk metals or metal oxides. In the cases of γ-Fe_2O_3, α-Fe_2O_3, V_2O_5, Au, Pd and Pt commercially acquired samples were used. The suppliers and purities of the used samples are listed in Table S1 in the Supplementary information. In the cases of CeO_2, Co_3O_4, MnO_x, ZnO, CuO, Cr_2O_3 and TiO_2 the oxide samples were prepared by flame spray pyrolysis according to the method described elsewhere [23]. This preparation method results in highly crystalline non-porous nanoparticles [34]. Catalyst precursors (Supplementary information, Table S2) at a total metal concentration of 0.25 M and 2-ethylhexanoic acid (Sigma Aldrich, ≥99%) at a concentration of 1.0 M were dissolved in toluene (Sigma Aldrich, anhydrous, ≥99.8%). The precursor solution was by means of a syringe pump delivered through a capillary (0.4 mm i.d.) into the flame at a rate of 3 mL/min, dispersed by a 5 NL/min O_2 flow and ignited by an annular 1 NL/min CH_4, 3 NL/min O_2 support flame (with NL referring to 298.15 K and 1 bar). The produced particles were with the aid of a vacuum pump collected on a water-cooled glass fiber filter (Whatman GF6, Ø = 240 mm) 45 cm above the burner nozzle. The powder was then sieved to <600 μm in order to avoid the presence of filter fibers in the product. In the cases of the flame made chromium and manganese oxides the flame made samples were relatively amorphous, and prior to use the samples were calcined (2 h 500 °C, 10 °C/min) in order to convert samples into more crystalline materials identifiable by XRD.

2.2. SiO_2 supported Fe-Cr binary oxide catalyst

To investigate the properties of binary oxide catalysts a series of SiO_2 supported $Fe_xCr_yO_z$ catalysts were prepared. SiO_2 extrudates (Saint-Gobain, 250 m^2/g) were impregnated with an aqueous solution of $Fe(NO_3)_3{\cdot}9H_2O$ and $Cr(NO_3)_3{\cdot}9H_2O$ (Sigma Aldrich) to produce $Fe_xCr_yO_z/SiO_2$ with a total metal loading of 0.00278 mol/g (15 wt% metal for an $FeCrO_x/SiO_2$ catalyst). The impregnated samples were aged for 2 h and then dried at 110 °C overnight. The dried catalyst precursors were then calcined in stagnant air for 2 h at 500 °C (ramp: 20 °C/min). Finally the calcined catalysts were crushed to <300 μm and then used in the powdered form.

2.3. Catalyst characterization

The specific surface areas of the catalyst samples were determined by nitrogen adsorption at liquid nitrogen temperature by means of a QuantaChrome Autosorb iQ_2 gas sorption analyzer. The specific surface area was determined through a 7-point, linear BET plot in the range of p/p_0 = 0.05–0.3. Prior to the BET measurement the sample was dried/degassed in flowing nitrogen at 170 °C for 2 h.

The identities of the various metal or metal oxide catalysts samples were verified by X-ray diffraction (XRD). XRD was measured with a PANalytical X'Pert PRO diffractometer with a Cu-Kα X-ray source operated at 45 kV and 40 mA and with a Ni-filter and automatic anti-scatter and divergence slits. Diffractograms were recorded between 2θ = 10° and 2θ = 80° with a step width of 2θ = 0.0130°.

2.4. Catalytic soot oxidation

The catalytic activity in soot oxidation was measured using a flow reactor setup. For the activity tests soot (~2 mg) and catalyst in a ratio of 1:5 (wt:wt) were stirred together with a spatula (loose contact) or crushed together for 6 min in an agate mortar (tight contact). In a few cases, where silica supported Fe-Cr binary oxide catalysts were tested, a higher soot:catalyst ratio of 1:10 (wt:wt) was used due to the lower fraction (15 wt%) of active material in these samples. The soot/catalyst mixture was transferred to a 7 cm long, 1 cm wide alumina sample holder, which was placed in the center of a quartz tube (length: 65 cm, inner diameter: 24 mm) within a horizontal, tubular furnace. The sample was then subjected to a 1 NL/min flow of 10.2 vol% O_2 in N_2. The feed gases (technical grade N_2 and O_2 from AGA A/S) were dosed by means of Bronkhorst EL-FLOW mass flow controllers. When the sample had been installed in the oven, and once any remnants of air had been purged from the reactor (once the CO_2 signal had fallen below the detection limit) the reactor was heated at a rate of 11 °C/min to a final temperature of 750 °C. The temperature was monitored by a type K thermoelement at the external surface of the quartz tube wall. The concentrations of CO and CO_2 in the reactor effluent were monitored continuously using an ABB AO2020 IR gas analyzer calibrated using a certified $CO/CO_2/N_2$ gas mixture from AGA A/S. During the experiments the levels of CO and CO_2 in the effluent stream were in the 0–500 ppmv range, and the oxygen conversion was thus negligible in the present experiments. For that reason the oxygen concentration dependence was omitted in the kinetic analyses of the results.

The reactivity of diesel soot can vary widely with parameters such as the engine type [35], the fuel type [36,37], the engine load [38,39] and the presence of catalytically active ash species [40,41]. Numerous different types of soot are used in the oxidation studies in the literature, and the rate of catalytic soot oxidation scales with the inherent reactivity of the soot [23]. The soot used in the experiments was a reference material from NIST: "SRM 2975 Diesel Particulate Matter" (from an Industrial Forklift). Various characterizations of this carbonaceous material can be found in the literature [23,42–44].

2.5. Kinetic analysis

The results have been interpreted in terms of a global kinetic model fitted to the data across the full conversion range in the temperature programmed reaction tests:

$$\frac{dX}{dt} = k_{cat.}(1-X)^n + k_{non-cat.}(1-X)^n = A_{cat.}\exp\left(\frac{-E_{a,cat.}}{RT}\right)(1-X)^n + A_{non-cat.}\exp\left(\frac{-E_{a,non-cat.}}{RT}\right)(1-X)^n$$

where X is the degree of carbon conversion (obtained from numerical integration of the CO and CO_2 signals), k is the rate constant, A is the pre-exponential factor, E_a is the apparent activation energy, and n is the reaction order in carbon. In this model the catalytic and the non-catalytic oxidation are treated as two parallel reactions. The kinetic parameters for the non-catalytic reaction, which are given the subscript "non-cat." in the equation above, are determined from oxidation experiments in the absence of a catalyst. The reaction order in carbon was chosen to give the best fit to the data across all the tested samples (both loose and tight contact). The

kinetic parameters are listed in Tables S5–S7 in the Supplementary information. The rate constant for the catalytic oxidation is used as a measure of catalytic activity that is independent of the degree of conversion and, after appropriate normalization by the surface area, also independent of the surface area of the catalyst. An evaluation of the present results in terms of the temperature of maximal oxidation rate (the optimum between the increase in reaction rate with temperature and the decline in reaction rate with increasing reactant consumption), which is another common measure of activity in soot oxidation, yields the same general conclusions, and such an analysis is provided in the Supplementary information (Figs. S8–S10).

2.6. Sources for the heat of oxygen chemisorption

The heats of chemisorption employed in this work have been obtained from the literature. For metal surfaces these values are generally heats of adsorption measured by calorimetry, and for metal oxides these values are generally heats of desorption determined from desorption data using the Clausius-Clapeyron equation. The heats of adsorption and desorption should be numerically identical under the assumption that adsorption and desorption occur by the same mechanism [45].

For metal oxides the heat of oxygen desorption from the surface generally depends strongly on the coverage. If the surface of an oxide equilibrated in an oxidizing atmosphere is partially reduced the heat of desorption of the remaining oxygen increases significantly [24,30]. The presently employed heats of desorption for metal oxides generally correspond to the most weakly adsorbed oxygen (the differential heat) on surfaces equilibrated in an oxidizing atmosphere at 500 °C. The heats of desorption for polycrystalline Co_3O_4, Fe_2O_3, Cr_2O_3 and TiO_2 were obtained from Boreskov et al. [24] while the heats of desorption for polycrystalline CuO and ZnO were obtained from Marshneva and Boreskov [28]. Isotopic exchange studies have suggested [46] that γ-Fe_2O_3 and α-Fe_2O_3 may differ in terms of the heat of chemisorption, but presently we have tentatively assigned them the same value, as γ-Fe_2O_3 has been observed to exhibit an α-Fe_2O_3-like surface in an oxidizing atmosphere [47]. In the case of manganese oxide it is difficult to prepare a completely phase pure sample. We have employed a heat of desorption of 92 kJ/mol reported for Mn_2O_3 [28]. Very similar values have been reported for other phases such as MnO_2 [24] and MnO [45]. and the employed value is therefore expected to be reasonably representative for the manganese oxide system. The employed heats of desorption for the various metal oxides are in good agreement with the Brønsted-Evans-Polanyi [48,49] relationship for isotopic $^{16}O_2/^{18}O_2$ exchange reported by Boreskov [46]. No direct measurement of the heat of oxygen desorption for CeO_2 could be found. Instead the heat of desorption for CeO_2 was estimated from the reported 67 kJ/mol activation energy in isotopic $^{16}O_2/^{18}O_2$ exchange [50] according to the Brønsted-Evans-Polanyi relationship obtained by Boreskov [46]. However, it must be added that significant ambiguity exists for exchange on ceria with reported activation energies in the 67–131 kJ/mol range [29,50–52]. In the case of V_2O_5 the heat of chemisorption is assumed equal to the desorption activation energy from Dziembaj [53], but this value must also be regarded with some caution, as there is significant ambiguity in the literature concerning the heat of oxygen chemisorption on V_2O_5 with reported values covering the wide range of 40–250 kJ/mol [24,28,53,54]. These variations have been ascribed to a strong dependence on the exact stoichiometry of the sample [53] and to the multiple solid phases in the vanadium-oxygen system, which is a challenge for the measurement of the heat of desorption [54,55].

An unresolved question is whether the surface oxygen in metal oxides that is probed by the heat of chemisorption (which is typically determined by desorption studies) is to be characterized as terminal lattice oxygen or as adsorbed oxygen or contains contributions from both—something that has also been discussed elsewhere [54,56]. Boreskov [56] made the reconciliatory point that for oxides with a surface composition equilibrated in an oxidizing atmosphere the rate of catalytic $^{18}O_2/^{16}O_2$ exchange is very similar to the rate of isotopic exchange with the oxygen of the oxide. This could suggest that adsorbed oxygen and lattice oxygen have similar reactivity or that activated, chemisorbed oxygen can exchange very rapidly with lattice oxygen in the oxide surface [56]. In this case the heat of oxygen chemisorption should at least be descriptive for both types of species.

Another question has been whether the heat of desorption describes a dissociated or molecular oxygen species. The best indication of an answer seems to come from the studies of oxygen desorption from α-Fe_2O_3 by Yang and Kung [57], which led the authors to conclude that the oxygen species probed by the presently used heat of desorption [24] was a dissociated species.

For the metals the oxygen binding energy is also highly dependent on the coverage with the heat of adsorption decreasing strongly with increasing coverage. As the exact coverages at reaction conditions are not known, heats of chemisorption corresponding to intermediate coverages have been chosen. For palladium a value of 150 kJ/mol, which corresponds to an intermediate coverage for both Pd(111) and for 4 nm Pd nanoparticles [58], has been selected. For platinum a heat of adsorption of 140 kJ/mol has been selected. This value corresponds to a moderately high coverage on Pt(111) [59,60] and is reasonably representative for a high coverage on Pt(110) [61]. In the case of gold the dependence of the catalytic properties on the particle size is well established [62–64]. Saliba et al. [65] summarized the available experimental evidence and came to the conclusion that dissociative adsorption of oxygen is endothermic on Au(111). Theoretical studies have reproduced the endothermic dissociative adsorption on Au(111), and have indicated that dissociative adsorption is almost thermoneutral on stepped and strained gold surfaces [64,66,67]. Presently the oxygen adsorption on gold is tentatively assigned as thermoneutral. This is also relatively close to the heat of decomposition of bulk Au_2O_3 [68,69].

3. Results and discussion

3.1. The materials

The identities of the employed catalytic materials have been verified by XRD. The diffraction patterns are shown in Figs. S1–S6 in the Supplementary information. The materials are generally phase pure with the exception of MnO_x and to a minor extent TiO_2. The MnO_x sample shows signs of several different phases (MnO_2, Mn_2O_3 and Mn_3O_4). The TiO_2 sample is primarily in the anatase phase, but minor traces of a rutile phase is visible. The surface areas of the employed catalysts have been determined by BET measurements and are listed in Table S3 in the Supplementary information. Across all the tested samples (loose contact, tight contact and non-catalytic oxidation) the best fit for the simple kinetic model was achieved with a carbon reaction order of $n = 2/3$. This is consistent with the soot particles behaving as uniformly shrinking spheres [70]. However, as discussed elsewhere [71], other situations could lead to similar reaction orders.

The non-catalytic soot oxidation occurs with an activation energy of 198.5 kJ/mol. This value is relatively high compared to reported activation energies for O_2 dissociation on defected graphite [72], but in the low end of the reported activation energies for CO and CO_2 desorption from semi-quinone and lactone species in graphite surfaces [72–74]. It is therefore difficult on this basis to

unambiguously assign a rate limiting step for the non-catalytic oxidation. In the non-catalytic oxidation 65% of the carbon is released as CO (see Fig. S13 in the Supplementary information). Such a preference for CO rather than CO_2 is also commonly observed in TPD of oxygen treated graphite surfaces [75–78]. The catalytic oxidations mainly result in CO_2 rather than CO, and the CO/CO_2 distribution seems to depend more strongly on the catalyst than on the type of contact with the soot (Supplementary information, Fig. S13).

3.2. Catalytic oxidation in tight contact

In tight contact tests soot and catalyst are crushed together, and an extensive soot/catalyst interface is expected [15]. Fig. 1 shows the rate of soot oxidation as a function of temperature for oxidation in tight contact with various catalytic materials. The results in Fig. 1 illustrate that the catalysts vary widely in activity with the more active catalytic materials like Co_3O_4 and CeO_2 causing the oxidation at a substantially lower temperature than less active materials such as ZnO and TiO_2.

In tight contact oxidation the reaction most likely involves oxide lattice oxygen. For oxides such as CeO_2, MoO_3 and V_2O_5, where the diffusion of lattice oxygen in the bulk is known to be very rapid [46,56,79–81], isotopic labeling experiments of carbon oxidation in tight contact with the oxide have shown a major involvement of bulk lattice oxygen [82–86]. TEM studies have also shown that the carbon consumption occurs at the soot/catalyst interface [87] and have provided indications of local ceria reduction associated with the soot oxidation [88]. The available observations thus indicate a reaction mechanism in tight contact that is of the type proposed by Mars and van Krevelen [89] with an initial reaction between carbon and surface lattice oxygen of the oxide followed by re-oxidation of the oxide by gas phase oxygen. It is reasonable that it in isotopic labeling experiments is the oxides for which bulk oxygen can most readily diffuse to a surface position that most clearly show an involvement of the lattice oxygen.

As the tight contact reaction is observed [87] to be focused at the soot/catalyst interface it seems appropriate to normalize the tight contact activity by the interfacial area. However, as it is difficult to assess the exact interfacial area in each case, the rate constants have been normalized by the maximally achievable initial interfacial area, which, depending of the respective surface areas, may be decided by either the soot or the catalyst. Here we thus assume a perfect dispersion of the solids and normalize the rate constant by the smallest surface area in the system (remembering the 1:5 ratio). Fig. 2 shows the fitted rate constant at a representative temperature of 400 °C for soot oxidation in tight contact with a catalyst as a function of the heat of oxygen chemisorption for the various catalytic materials.

Fig. 2 shows that the data outline what Balandin [90] termed a volcano curve with an optimal activity at an intermediate bond strength. As the heat of oxygen chemisorption decreases, oxygen is more easily released from the catalyst surface, and the oxidation activity increases. Eventually, in the case of gold, oxygen activation becomes such a limitation that this leads to a decreased activity. This is presumably especially clear for the employed bulk gold sample, which has a very low surface area (1.1 m^2/g). Small gold nanoparticles would be expected to bind oxygen more strongly [64] and thus have a more appropriate binding energy and higher activity, as it is also observed in graphite oxidation [91,92]. Among the tested materials, Co_3O_4 and CeO_2 are the catalysts closest to the optimal oxygen bond strength. V_2O_5 can be seen to be a positive outlier in Fig. 2. This may be related to the normalization of the rate constant by the surface area of the catalyst. The reaction occurs above the Tammann temperature of V_2O_5 (209 °C), and catalyst species could in principle wet the entire soot surface and create a larger interface than expected from the initial oxide surface area. MnO_x and Cr_2O_3 are negative outliers. For these materials a greater fraction of the carbon is released as CO than expected from the general tendency (see Fig. S13 in the Supplementary information). If the oxygen coverage for these materials is lowered under the reaction conditions this could also impact the activity for the two materials.

Fig. 3 shows the apparent activation energies for tight contact oxidation in the presence of the evaluated catalysts as a function of their heats of oxygen chemisorption. With approximation the data can be seen to follow a linear tendency—a so-called Brønsted-Evans-Polanyi [48,49] relationship. The slope of the Brønsted-Evans-Polanyi relationship is a measure of the extent to which the transition state resembles the final state (complete rupture of the oxygen-catalyst bond). Fig. 3 shows that the linear relationship has a slope of 0.32, indicating that the transition state, which Hennig [91] proposed to be a bridging metal-oxygen-carbon species, is closest to the initial state in character.

Fig. 4 outlines the possible steps of the reaction mechanism. Reaction R1 is the broadly supported mechanism for adsorption of oxygen on a metal oxide [93–95]. By electron donation from the metal the adsorbed oxygen becomes a superoxide (O_2^-), a peroxide (O_2^{2-}), dissociated atomic oxygen (O^-) and finally lattice oxygen (O^{2-}). Following Hennig's [91] proposal of a bridging metal-oxygen-carbon transition state lattice oxygen from the catalyst is then transferred to the carbonaceous material, in this case to form a semi-quinone species (R2). The reaction leaves a reduced surface site in the metal oxide, which is reoccupied according to R1. It is known from TPD studies [73,74] that the semi-quinone species can desorb as CO (R3), but the activation energy for desorption of CO_2 from carbon bound to two oxygen atoms is significantly lower [73,74], and, when possible, a second transfer of oxygen (R4) should be a more favourable pathway. In the catalytic oxidation the fraction of carbon released as CO is low compared to the non-catalytic oxidation (Supplementary information, Fig. S13), but as secondary catalytic oxidation of released CO is also a possibility, it is difficult to identify the immediate product of the carbon oxidation. It seems likely that the rate limiting step is one of the oxygen transfer reactions (R2 or R4), since the reaction rate depends on both the oxygen bond strength of the catalyst (Figs. 2 and 3) and the inherent reactivity of the soot [23].

3.3. Catalytic oxidation in loose contact

Fig. 5 shows the carbon oxidation rate as a function of temperature during oxidation of soot in loose contact with various catalytic materials. Fig. S11 in the Supplementary information also shows the corresponding carbon conversions as functions of temperature.

Fig. 5 illustrates that in loose contact the decrease in oxidation temperature due to the presence of a catalyst is less drastic than in the tight contact case, where the oxidation temperatures with different catalysts varied by several hundred degrees. Fig. 5 shows that at lower temperatures Co_3O_4 gives the highest rate. However, at higher temperatures oxidation in the presence of a material like Cr_2O_3 becomes relatively faster, and the conversion in the presence of Cr_2O_3 overtakes the conversion in the presence of Co_3O_4.

In loose contact the soot/catalyst interfacial area will be much smaller than the maximally achievable area due to the inferior mixing of the two components, and the interface is expected to be limited to the contact points between larger clusters of soot particles and larger clusters of catalyst particles [15]. It therefore does not seem descriptive to normalize the activity by the maximally achievable interfacial area as done in the case of tight contact. Furthermore there are, as described below, indications that in addition to the interface reaction important for tight contact oxidation (in loose contact the same interface reaction would still be expected to proceed at the limited number of contact points) there is another

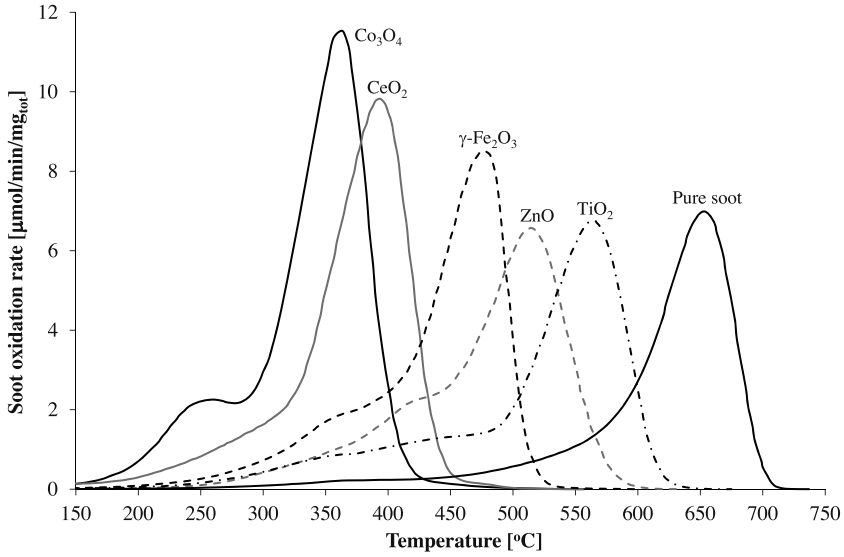

Fig. 1. The rates of carbon oxidation (normalized by the total, initial amount of carbon) in tight contact with various catalysts as functions of the temperature. Experimental conditions: Soot:Catalyst = 1:5 wt:wt, ramp = 11 °C/min, 1 NL/min, 10.2 vol% O_2 in N_2.

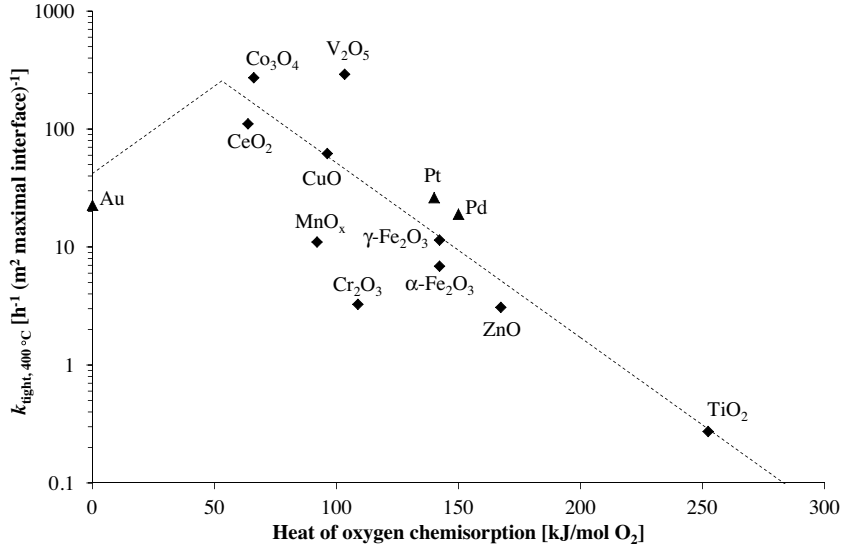

Fig. 2. The rate constant (at a representative temperature of 400 °C) for soot oxidation in tight contact with a catalyst as a function of the heat of oxygen chemisorption for various catalytic materials. The rate constant is normalized by the maximally achievable interfacial area (determined by the smallest surface area of either soot or catalyst). The dashed lines are given as a guide to the eye. With the available data it is difficult to identify the exact optimum of the volcano. The experimental conditions are given in connection with Fig. 1.

mechanism that contributes significantly to the oxidation in the loose contact tests.

For loose contact oxidation isotope labeling studies with CeO_2-based catalysts [96,97] have shown that the produced CO and CO_2 contain a significant fraction of lattice oxygen from the oxide catalyst, so the oxidation does seem to occur at least partly with oxygen originating on the catalyst surface. Zeng et al. [98] and Yamazaki et al. [97] studied catalytic soot oxidation with a catalyst separated from the soot by a layer of inert particles and found that the oxidation temperature depended upon the thickness of the inert layer. This could indicate a mechanism, where oxygen is activated on the catalyst and then diffuses to the soot and reacts (a type of spillover phenomenon [99]). For carbon oxidation by Cr_2O_3 TGA and microscopy experiments [92], IR studies [100], electron microscopy investigations [101] and isotopic labeling experiments [85] have also pointed to a mechanism where oxygen is activated on the catalyst and then diffuses to reactive sites on the carbon surface and reacts. The observation [97,98] that oxygen remains activated when transferred from the catalyst to the soot across a dividing layer of inert material seem most consistent with the activated oxygen species being dissociated atomic oxygen. Molecular species such as O_2^- and O_2^{2-} are activated by electron donation, while adsorbed on the catalyst, but would not necessarily be expected to carry this activation with them when removed from the catalyst surface and transferred across an inert surface to carbon. If the catalyst surface can create atomic oxygen, which can migrate to the carbon to react, this would be expected to accelerate the soot oxidation. Atomic oxygen has a relatively high reaction probability on graphite [102], and a neighboring catalyst dosing atomic oxygen should thus raise the oxygen coverage on the surface of the carbonaceous material [85]. This should benefit the oxidation rate, since the activation energies for desorption of CO and CO_2 from oxidized species in the surface of graphite decrease with increasing oxygen coverage [72,77,78,103,104].

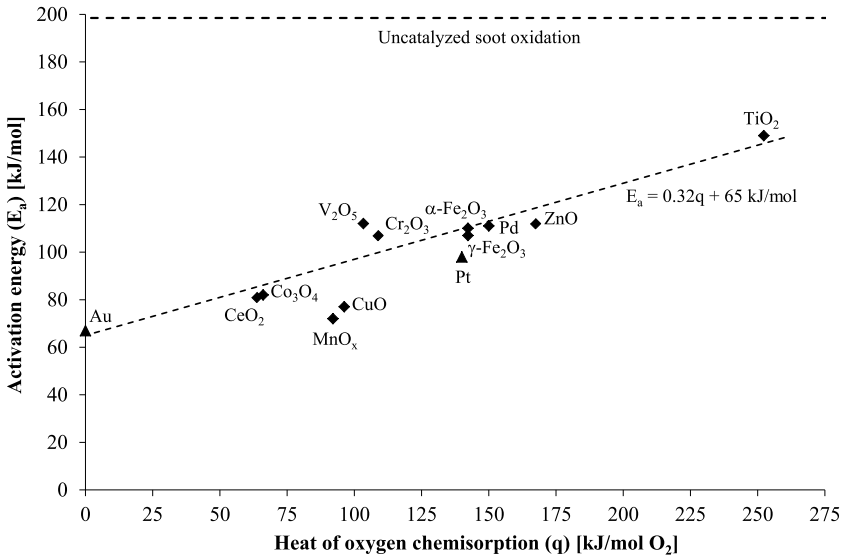

Fig. 3. Brønsted-Evans-Polanyi relationship between the apparent activation energy for soot oxidation in tight contact with a catalyst and the heat of oxygen chemisorption on the catalyst.

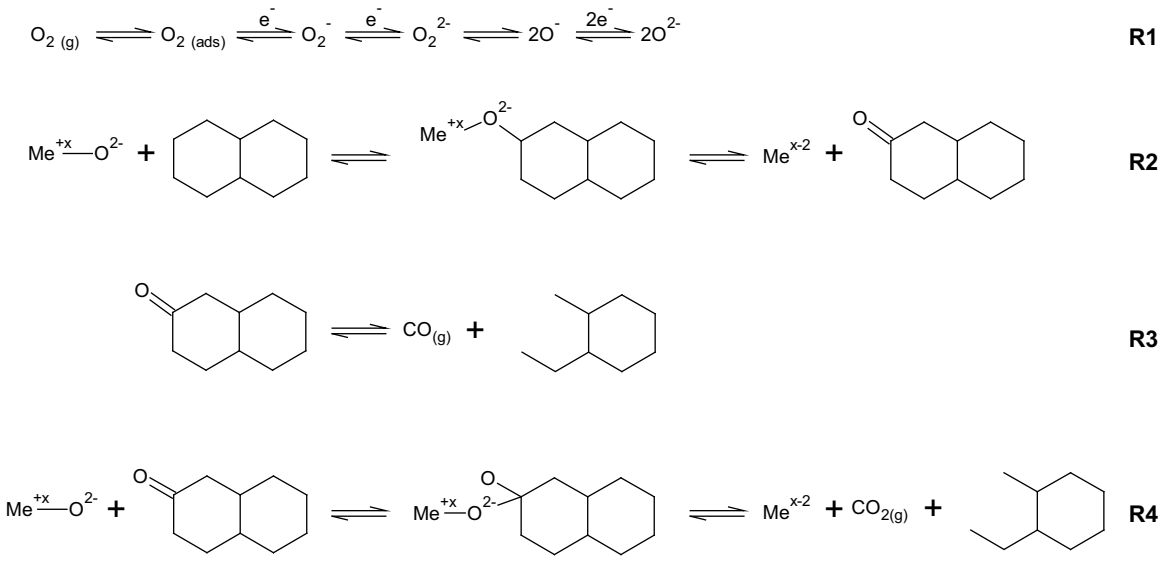

Fig. 4. Sketch of the possible structure of the reaction mechanism in tight contact soot oxidation. Me denotes a metal ion in the surface of the metal oxide. The double ring is here used to represent the carbonaceous material.

In the case of loose contact oxidation another part of the mechanism is thus expected to be the transfer of the activated oxygen species to the carbonaceous material. This transfer could, as suggested elsewhere [105,106], occur via the gas phase (possibly by evolution of O· radicals or derived O_3 from the catalyst surface), or via surface diffusion to the soot/catalyst interface and possibly onto the soot. In the latter case the heat of oxygen chemisorption on the catalyst would also be important for the transport, as the rate of surface diffusion of an adsorbate depends on its heat of chemisorption [107].

Assuming that the primary role of the catalyst is oxygen activation, and assuming that the number sites active for oxygen activation scales linearly with the total catalyst surface area it would seem most reasonable to normalize the determined rate constants by the total surface area of the catalyst (here the initial area is used). Furthermore, at the present state of knowledge on loose contact soot oxidation, where the active site for oxygen activation has not been unambiguously identified, a normalization of the catalytic activity by the total surface area of the bulk catalysts appears to be the best approach. Fig. 6 shows the fitted rate constants for soot oxidation in loose contact with a catalyst at a representative temperature of 600 °C as a function of the heat of oxygen chemisorption for various catalytic materials. Fig. 6 shows that the catalytic activities, also in the case of loose contact, outline a volcano curve with an optimal activity at intermediate bond strength. Among the materials evaluated Cr_2O_3 is the catalytic material closest to the optimal bond strength. The fact that the optimal oxygen bond strength has shifted compared to the tight contact oxidation could also suggest that there are differences in terms of the reaction mechanisms in the two cases.

A factor that must also be considered for the loose contact case is the impact of catalyst mobility at the high reaction temperatures. If catalyst species have substantial mobility due to a high volatility or a low melting point this will lead to establishment of additional soot/catalyst interface and thereby an increased effect of the catalyst [12,15,91,108–110]. As in the tight contact case the

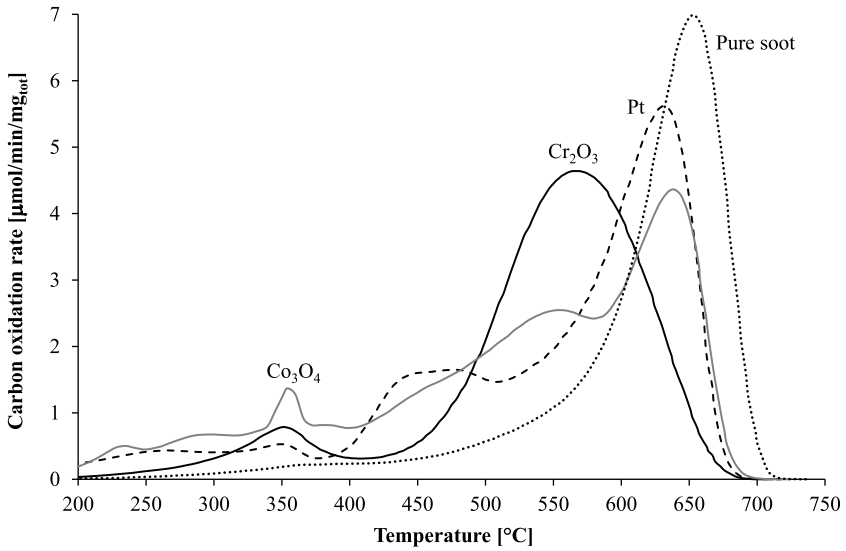

Fig. 5. The rates of carbon oxidation (normalized by the total, initial amount of carbon) in loose contact with various catalysts as a function of the temperature. Experimental conditions: Soot:Catalyst = 1:5 wt:wt, ramp = 11 °C/min, 1 NL/min, 10.2 vol% O_2 in N_2.

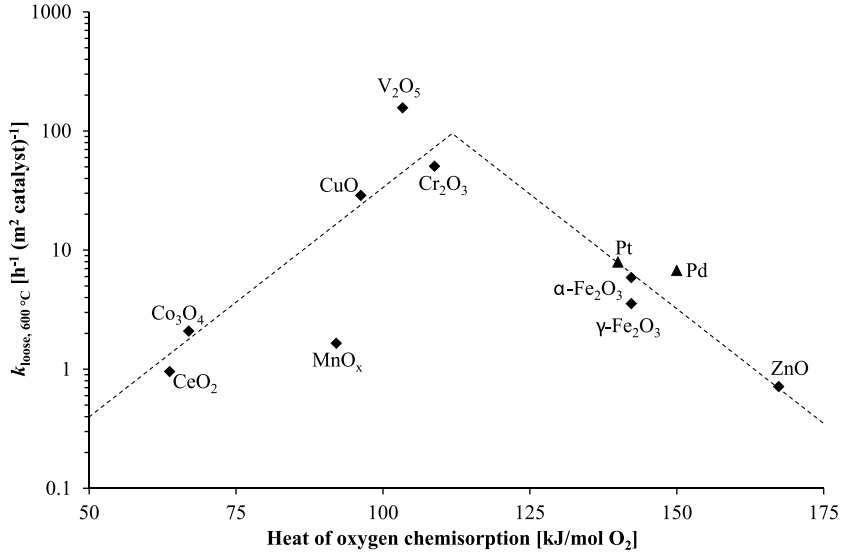

Fig. 6. The rate constant (at a representative temperature of 600 °C) for soot oxidation in loose contact with a catalyst as a function of the heat of oxygen chemisorption for various catalytic materials. The rate constant is normalized by the surface area of the catalyst. The experimental conditions are given in connection with Fig. 5.

activity of V_2O_5 is higher than expected from the general tendency in Fig. 6, but since the soot oxidation in loose contact occurs significantly above the Tammann temperature and in the last part of the test even above the melting point of V_2O_5, it could well be that catalyst species wet the entire soot surface, and the normalization of the rate constant by the initial catalyst surface area is thus not necessarily descriptive for this catalytic material (vanadium oxide was observed to have wetted the entire sample holder after the experiment).

Fig. 7 shows the Brønsted-Evans-Polanyi relationship for oxidation in loose contact. Again there is, with approximation, a linear relationship between activation energy and heat of chemisorption. However, there is some scattering of the data, perhaps as a result of a greater influence of non-catalytic oxidation and for some materials a smaller catalytic effect in the loose contact mode. Compared to the tight contact case the slope of the Brønsted-Evans-Polanyi line for loose contact is higher. This would suggest a transition state closer to the final state [111], namely a complete rupture of the oxygen-catalyst bond in the loose contact case.

Fig. 8 illustrates the presented mechanistic considerations for loose contact oxidation. Oxygen is activated by adsorption of the catalyst according to reaction R1. As discussed above it is possible that the loose contact oxidation involves a dissociated oxygen species. The activated oxygen then migrates (by surface diffusion or through the gas phase) to the surface of the carbonaceous material, where it creates an oxidized surface species, here again exemplified by a semi-quinone species (R5). As discussed in connection with the tight contact reaction CO can then desorb from the semi-quinone species (R3) [73,74]. Alternatively, an attack on the oxidized carbon atom by a second oxygen atom can result in the formation of CO_2 (R6).

A final point worth mentioning is that catalysts binding oxygen more weakly are not completely inactive in the loose contact oxidation. At lower temperatures the more weakly bound oxygen is more readily available (the activation energy is lower as seen in Fig. 7) and the catalytic rate obtained with Co_3O_4 is even higher than the one obtained with Cr_2O_3. However, at higher temperatures the activation of oxygen on the more weakly binding surface

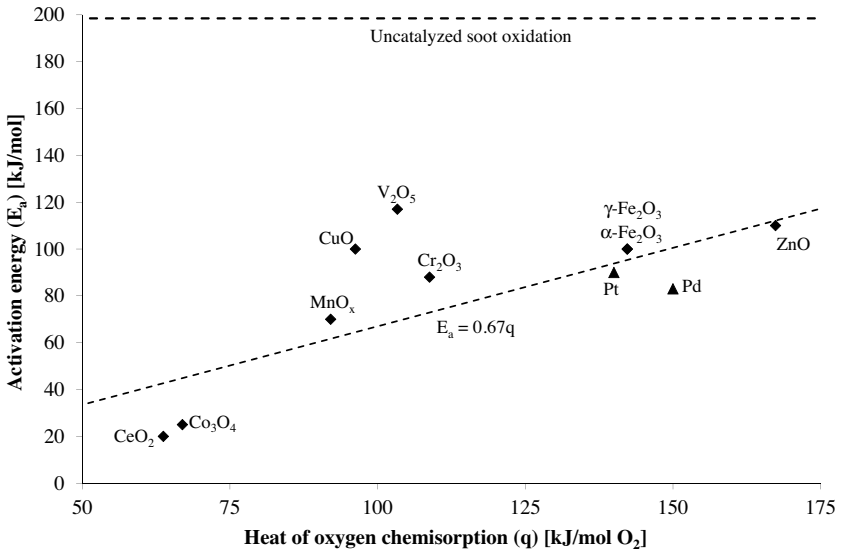

Fig. 7. Brønsted-Evans-Polanyi relationship between the apparent activation energy for soot oxidation in loose contact with a catalyst and the heat of oxygen chemisorption on the catalyst.

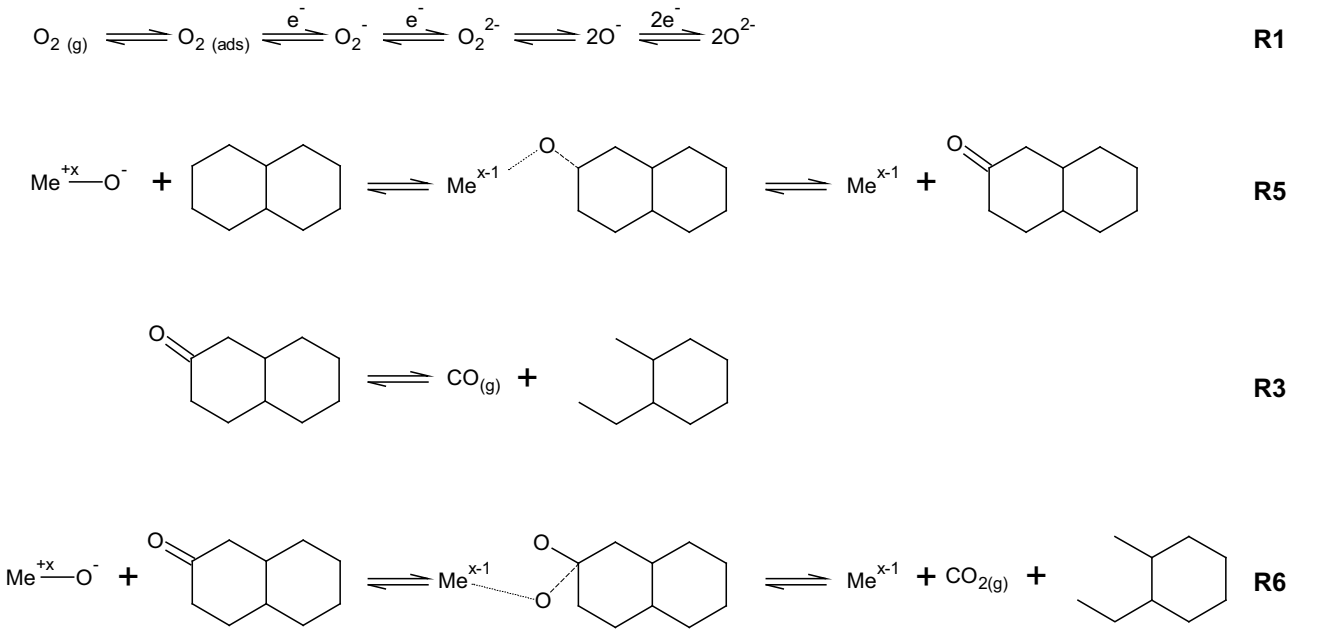

Fig. 8. Sketch of the possible structure of the reaction mechanism in loose contact soot oxidation. Me denotes a metal ion in the surface of the metal oxide. The double ring is here used to represent the carbonaceous material. The dashed lines are here used to indicate the migration of activated oxygen to the surface of the carbonaceous material as discussed in the text.

is presumably rate limiting compared to a surface that binds oxygen more strongly (such as Cr_2O_3), and the rate achieved with the more strongly binding catalysts overtakes the rate of the weakly binding catalyst.

3.4. Identification of an improved catalyst by an interpolation principle

Fig. 6 indicates that optimal loose contact activity corresponds to a material binding oxygen slightly stronger than Cr_2O_3, but less strongly than Fe_2O_3. From Balandin's [90] concept of the volcano curve comes also the interpolation principle—the idea that two materials, one on each side of the optimal bond strength, can be combined in a mixed phase with a more optimal binding energy. To test if this principle could be used as a guide in the identification of improved loose contact catalysts, a series of silica supported Fe-Cr binary oxides with varying composition was prepared. A supported system was chosen as a convenient way of preparing clusters of a mixed oxide or highly intermingled pure oxides. The XRD patterns of the binary Fe-Cr catalysts (Fig. S7 in the supplementary information) suggest a somewhat gradual transition from α-Fe_2O_3 to α-Cr_2O_3 in the binary oxides, which might indicate that mixed oxide phases were obtained. These silica supported $Fe_aCr_bO_x$ catalysts were tested for activity in soot oxidation with loose soot/catalyst contact, and Fig. 9 shows the rate constant normalized by the amount of active metals as a function of the iron fraction in the binary oxides. Fig. 9 illustrates that the activity of the catalysts in fact passes through an optimum for an $FeCr_2O_x$ cat-

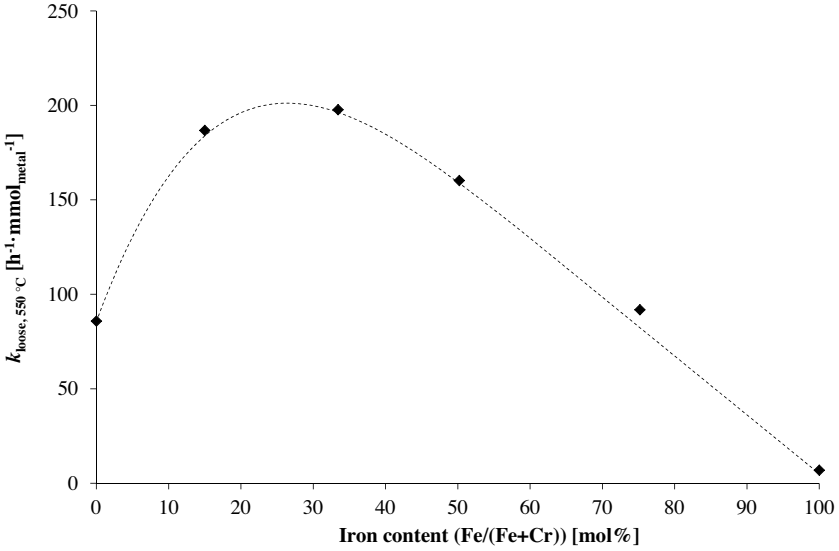

Fig. 9. The rate constant (at a representative temperature of 550 °C) for soot oxidation in loose contact with $Fe_aCr_bO_x/SiO_2$ as a function of the iron fraction [Fe/(Cr + Fe)] in the binary oxides. Experimental conditions: Soot:Catalyst = 1:10 wt:wt, ramp = 11 °C/min, 1 NL/min, 10.2 vol% O_2 in N_2.

alyst (33 mol% Fe), which at 550 °C has a rate constant 2.3 times higher than pure α-Cr_2O_3 and 29 times higher than pure α-Fe_2O_3, and it is promising to observe that more active multi-component catalysts can be developed by interpolation principles.

4. Conclusion

The oxygen bond strength on the surface of a catalyst as measured by the heat of oxygen chemisorption is observed to be a very important parameter for the activity of the catalyst in soot oxidation. With both intimate contact between soot and catalyst (tight contact) and with the solids stirred loosely together (loose contact) the rate constants (for a reaction order of 2/3 in carbon) of a number of catalytic materials outline a volcano curve when depicted against their heats of oxygen chemisorption. However, the optima of the volcano curves correspond to different heats of chemisorption for the two contact types. This could be related to mechanistic differences between the oxidation in the two situations. Among the tested metal or metal oxide catalysts Co_3O_4 and CeO_2 were nearest to the optimal bond strength in tight contact oxidation, while Cr_2O_3 was nearest to the optimum in loose contact oxidation. For both the tight and loose contact tests the activation energies for soot oxidation with the different catalytic materials formed linear Brønsted-Evans-Polanyi relationships with the heat of oxygen chemisorption on the catalytic materials, but the slopes of the Brønsted-Evans-Polanyi relationships differ between the tight and loose contact cases. The optimum of the volcano curve in loose contact occurs between the oxygen bond strengths of α-Fe_2O_3 and α-Cr_2O_3. From an interpolation principle it might thus be expected that $Fe_aCr_bO_x$ binary oxides could exhibit improved activity compared to the pure oxides, and this was also observed, as a silica supported $FeCr_2O_x$ catalyst had a rate constant at 550 °C that was 2.3 times higher than the rate constant of a pure Cr_2O_3/SiO_2 catalyst and 29 times higher than the one for a pure Fe_2O_3/SiO_2 catalyst.

Acknowledgements

Financial support from The Danish Council for Strategic Research (DSF) is gratefully acknowledged (Grant No. 2106-08-0039). We thank Helge Kildahl Rasmussen from DTU Physics for aid in connection with the XRD measurements.

Appendix A. Supplementary data

Supplementary data associated with this article can be found, in the online version, at http://dx.doi.org/10.1016/j.apcatb.2016.01.068.

References

[1] C. Ris, Inhal. Toxicol. 19 (2007) 229–239.
[2] W.L. Chameides, M. Bergin, Science 297 (2002) 2214–2215.
[3] R.A. Kerr, Science 339 (2013), 382–382.
[4] B. Frank, M. Schuster, R. Schlögl, D.S. Su, Angew. Chem. Int. Ed. 52 (2013) 2673–2677.
[5] D.B. Kittelson, J. Aerosol Sci. 29 (1998) 575–588.
[6] M.O. Andreae, V. Ramanathan, Science 340 (2013) 280–281.
[7] B.A.A.L. Van Setten, M. Makkee, J.A. Moulijn, Catal. Rev. Sci. Eng. 43 (2001) 489–564.
[8] J. Neeft, M. Makkee, J.A. Moulijn, Fuel Process. Technol. 47 (1996) 1–69.
[9] J. Adler, Int. J. Appl. Ceram. Technol. 2 (2005) 429–439.
[10] A.M. Stamatelos, Energy Convs. Manage. 38 (1997) 83–99.
[11] B.W.L. Southward, S. Basso, SAE paper 2008-01-0481, (2008).
[12] J. Neeft, M. Makkee, J.A. Moulijn, Chem. Eng. J. 64 (1996) 295–302.
[13] J. Neeft, M. Makkee, J.A. Moulijn, Appl. Catal. B 8 (1996) 57–78.
[14] J. Neeft, O.P. van Pruissen, M. Makkee, J.A. Moulijn, Stud. Surf. Sci. Catal. 96 (1995) 549–561.
[15] D. Gardini, J.M. Christensen, C.D. Damsgaard, A.D. Jensen, J.B. Wagner, Appl. Catal. B 183 (2016) 28–36.
[16] A.G. Konstandopoulos, S. Lorentzou, C. Pagkoura, K. Ohno, K. Ogyu, T. Oya, SAE paper 2007-01-1950, (2007).
[17] A.G. Konstandopoulos, E. Papaioannou, Kona 26 (2008) 36–65.
[18] A. Konstandopolous, E. Papaioannou, D. Zarvalis, S. Skopa, P. Baltzopoulou, E. Kladopoulou, M. Kostoglou, S. Lorentzou, SAE paper 2005-01-0670, (2005).
[19] P.A. Kumar, M.D. Tanwar, S. Bensaid, N. Russo, D. Fino, Chem. Eng. J. 207–208 (2012) 258–266.
[20] P. Doggali, H. Kusaba, S. Rayalu, Y. Teraoka, N. Labhsetwar, Top. Catal. 56 (2013) 457–461.
[21] Q. Liang, X. Wu, X. Wu, D. Weng, Catal. Lett. 119 (2007) 265–270.
[22] K. Shimizu, H. Kawachi, A. Satsuma, Appl. Catal. B 96 (2010) 169–175.
[23] J.M. Christensen, D. Deiana, J.-D. Grunwaldt, A.D. Jensen, Catal. Lett 144 (2014) 1661–1666.
[24] G.K. Boreskov, V.V. Popovsky, V.A. Sazonov, In: J.W. Hightower (ed.) Fourth Int. Cong. Catal.—Reprints of Papers, vol. 2 (1968), pp. 580–603.
[25] V.A. Roiter, G.I. Golodets, Y.I. Pyatnitzky, In: J.W. Hightower (ed.) Fourth Int. Cong. Catal.—Reprints of Papers, vol. 2 (1968), pp. 628–648.
[26] K. Klier, J. Catal. 8 (1967) 14–21.
[27] V.V. Popovskii, Theor. Exp. Chem. 5 (1972) 475–476.
[28] V.I. Marshneva, G.K. Boreskov, React. Kinet. Catal. Lett. 1 (1974) 15–19.
[29] G.K. Boreskov, L.A. Kasatkina, Russ. Chem. Rev. 37 (1968) 613–628.
[30] V.A. Razdobarov, V.A. Sadykov, S.A. Veniaminov, N.N. Bulgakov, O.N. Kovalenko, Y.D. Pankratiev, V.V. Popovskii, G.N. Kryukova, S.F. Tikhov, React. Kinet. Catal. Lett. 37 (1988) 109–114.

[31] Y. Martynova, S. Shaikhutdinov, H.-J. Freund, ChemCatChem 5 (2013) 2162–2166.
[32] W.M.H. Sachtler, G.J.H. Dorgelo, J. Fahrenfort, R.J.H. Voorhoeve, In: J.W. Hightower (ed.) Fourth Int. Cong. Catal.—Reprints of Papers, vol. 2, (1968), pp. 604–627.
[33] G.I. Golodets, Theor. Exp. Chem. 18 (1982) 27–34.
[34] R. Strobel, A. Baiker, S.E. Pratsinis, Adv. Powder Technol. 17 (2006) 457–480.
[35] D.S. Su, J.-O. Müller, R.E. Jentoft, D. Rothe, E. Jacob, R. Schlögl, Top. Catal. 30/31 (2004) 241–245.
[36] H. Jansma, D. Fino, R. Uitz, M. Makkee, Ind. Eng. Chem. Res. 51 (2012) 7559–7564.
[37] A.L. Boehman, J. Song, M. Alam, Energy Fuels 19 (2005) 1857–1864.
[38] K.J. Higgins, H. Jung, D.B. Kittelson, J.T. Roberts, M.R. Zachariah, Environ. Sci. Technol. 37 (2003) 1949–1954.
[39] A. Setiabudi, M. Makkee, J.A. Moulijn, Appl. Catal. B 50 (2004) 185–194.
[40] H. Jung, D.B. Kittelson, M.R. Zachariah, Combust. Flame 142 (2005) 276–288.
[41] H. Jung, D.B. Kittelson, M.R. Zachariah, SAE paper 2003-01-3179, (2003).
[42] J. Im, C.M. Lee, J.T. Coates, Chemosphere 71 (2008) 621–628.
[43] A. Braun, B.S. Mun, F.E. Huggins, G.P. Huffman, Environ. Sci. Technol. 41 (2007) 173–178.
[44] Ö. Gustafsson, T.D. Bucheli, Z. Kukulska, M. Andersson, C. Largeau, J.-N. Rouzaud, C.M. Reddy, T.I. Eglinton, Global Biogeochem. Cycles 15 (2001) 881–890.
[45] D.O. Hayward, B.M.W. Trapnell, Chemisorption, 2nd ed., Butterworths, London, 1964.
[46] G.K. Boreskov, V.S. Muzykantov, Ann. N. Y. Acad. Sci. 213 (1973) 137–170.
[47] M. Bowker, G. Hutchings, P.R. Davies, D. Edwards, R. Davies, S. Shaikhutdinov, H.-J. Freund, Surf. Sci. 606 (2012) 1594–1599.
[48] M.G. Evans, M. Polanyi, Trans. Faraday Soc. 34 (1938) 11–24.
[49] J.N. Brønsted, K. Pedersen, Z. Phys. Chem. 108 (1924) 185–235.
[50] G.V. Antoshin, K.M. Minachev, R.V. Dmitriev, Bull. Acad. Sci. USSR 16 (1967) 1793–1795.
[51] D. Martin, D. Duprez, J. Phys. Chem. 100 (1996) 9429–9438.
[52] E.R.S. Winter, J. Chem. Soc. A 288 (1968) 9–290 (2).
[53] R. Dziembaj, React. Kinet. Catal. Lett. 9 (1979) 389–393.
[54] R. Dziembaj, J. Solid State Chem. 26 (1978) 167–171.
[55] R. Dziembaj, J. Solid State Chem. 26 (1978) 159–165.
[56] G.K. Boreskov, Adv. Catal. 15 (1964) 285–339.
[57] B.L. Yang, H.H. Kung, J. Catal. 75 (1982) 329–336.
[58] M. Peter, J.M. Flores Camacho, S. Adamovski, L.K. Ono, K.-H. Dostert, C.P. O'Brien, B. Roldan Cuenya, S. Schauermann, H.-J. Freund, Angew. Chem. Int. Ed. 52 (2013) 5175–5179.
[59] Y.Y. Yeo, L. Vattuone, D.A. King, J. Chem. Phys. 106 (1997) 392–401.
[60] D.H. Parker, M.E. Bartram, B.E. Koel, Surf. Sci. 217 (1989) 489–510.
[61] C.E. Wartnaby, A. Stuck, Y.Y. Yeo, D.A. King, J. Phys. Chem. 100 (1996) 12483–12488.
[62] M. Haruta, N. Yamada, T. Kobayashi, S. Iijima, J. Catal. 115 (1989) 301–309.
[63] M. Haruta, Catal. Today 36 (1997) 153–166.
[64] N. Lopez, T.V.W. Janssens, B.S. Clausen, Y. Xu, M. Mavrikakis, T. Bligaard, J.K. Nørskov, J. Catal. 223 (2004) 232–235.
[65] N. Saliba, D.H. Parker, B.E. Koel, Surf. Sci. 410 (1998) 270–282.
[66] M. Mavrikakis, P. Stoltze, J.K. Nørskov, Catal. Lett. 64 (2000) 101–106.
[67] Y. Xu, M. Mavrikakis, J. Phys. Chem. B 107 (2003) 9298–9307.
[68] H. Tsai, E. Hu, K. Perng, M. Chen, J.-C. Wu, Y.-S. Chang, Surf. Sci. 537 (2003) L447–L450.
[69] S.J. Ashcroft, E. Schwarzmann, J. Chem. Soc. Faraday Trans. 1 68 (1972) 1360–1361.
[70] O. Levenspiel, The Chemical Reactor Omnibook, OSU Book Stores Corvallis, Oregon, 1979.
[71] C.J. Tighe, M.V. Twigg, A.N. Hayhurst, J.S. Dennis, Combust. Flame 159 (2012) 77–90.
[72] S.R. Kelemen, H. Freund, Carbon 23 (1985) 619–625.
[73] B. Marchon, J. Carrazza, H. Heinemann, G.A. Somorjai, Carbon 26 (1988) 507–514.
[74] B. Marchon, W.T. Tysoe, J. Carrazza, H. Heinemann, G.A. Somorjai, J. Phys. Chem. 92 (1988) 5744–5749.
[75] S.S. Barton, G.L. Boulton, B.H. Harrison, Carbon 10 (1972) 395–400.
[76] S.R. Kelemen, H. Freund, Energy Fuels 2 (1988) 111–118.
[77] S.S. Barton, B.H. Harrison, J. Dollimore, J. Phys. Chem. 82 (1978) 290–294.
[78] S.S. Barton, B.H. Harrison, J. Dollimore, J. Chem. Soc. Faraday Trans. 1 69 (1973) 1039–1048.
[79] W.C. Cameron, A. Farkas, L.M. Litz, J. Phys. Chem. 57 (1953) 229–238.
[80] D.G. Klissurski, R.A. Ross, T.J. Griffith, Can. J. Chem. Eng. 52 (1974) 3847–3851.
[81] K. Hirota, Y. Kera, S. Teratani, J. Phys. Chem. 72 (1968) 3133–3141.
[82] M. Machida, Y. Murata, K. Kishikawa, D. Zhang, K. Ikeue, Chem. Mater. 20 (2008) 4489–4494.
[83] A. Bueno-Lopez, K. Krishna, M. Makkee, J. Moulijn, J. Catal. 230 (2005) 237–248.
[84] A. Bueno-López, K. Krishna, M. Makkee, J.A. Moulijn, Catal. Lett. 99 (2005) 203–205.
[85] G. Mul, F. Kapteijn, C. Doornkamp, J.A. Moulijn, J. Catal. 179 (1998) 258–266.
[86] K. Harada, T. Oishi, S. Hamamoto, T. Ishihara, J. Phys. Chem. C 118 (2013) 559–568.
[87] S. Simonsen, S. Dahl, E. Johnson, S. Helveg, J. Catal. 255 (2008) 1–5.
[88] E. Aneggi, N.J. Divins, C. de Leitenburg, J. Llorca, A. Trovarelli, J. Catal. 312 (2014) 191–194.
[89] P. Mars, D.W. Van Krevelen, Chem. Eng. Sci. Special Suppl. 3 (1954) 41–59.
[90] A.A. Balandin, Adv. Catal. 19 (1969) 1–210.
[91] G.R. Hennig, J. Inorg. Nucl. Chem. 24 (1962) 1129–1137.
[92] D.W. McKee, Carbon 8 (1970) 623–635.
[93] V.A. Shvets, V.B. Kazansky, J. Catal. 25 (1972) 123–130.
[94] M. Che, A.J. Tench, Adv. Catal. 31 (1983) 77–133.
[95] C. Li, K. Domen, K. Maruya, T. Onishi, J. Am. Chem. Soc. 111 (1989) 7683–7687.
[96] K. Suzuki, K. Harada, H. Yamada, K. Okamoto, A. Takami, SAE paper 2007-01-1919, (2007).
[97] K. Yamazaki, Y. Sakakibara, F. Dong, H. Shinjoh, Appl. Catal. A 476 (2014) 113–120.
[98] L. Zeng, T. Turek, A.P. Weber, Chem. Ing. Tech. 83 (2011) 1276–1281.
[99] E. Baumgarten, A. Schuck, Appl. Catal. 37 (1988) 247–257.
[100] G. Mul, J.P.A. Neeft, F. Kapteijn, J.A. Moulijn, Carbon 36 (1998) 1269–1276.
[101] R.T.K. Baker, J.J. Chludzinski, Carbon 19 (1981) 75–82.
[102] H.D. Allendorf, D.E. Rosner, AIAA J. 6 (1968) 650–654.
[103] Z.H. Zhu, J. Finnerty, G.Q. Lu, R.T. Yang, Energy Fuels 16 (2002) 1359–1368.
[104] P.L. Walker, R.L. Taylor, J.M. Ranish, Carbon 29 (1991) 411–421.
[105] L. Zeng, A.P. Weber, Chem. Ing. Tech. 84 (2012) 295–300.
[106] E. Baumgarten, A. Schuck, React. Kinet. Catal. Lett. 62 (1997) 209–216.
[107] K.J. Sladek, E.R. Gilliland, R.F. Baddour, Ind. Eng. Chem. Fundam. 13 (1974) 100–105.
[108] D. Fino, N. Russo, C. Badini, G. Saracco, V. Specchia, AIChE J. 49 (2003) 2173–2180.
[109] G. Mul, J. Neeft, F. Kapteijn, M. Makkee, J.A. Moulijn, Appl. Catal. B 6 (1995) 339–352.
[110] W.L. Holstein, M. Boudart, Fuel 62 (1983) 162–165.
[111] J.K. Nørskov, T. Bligaard, A. Logadottir, S. Bahn, L.B. Hansen, M. Bollinger, H. Bengaard, B. Hammer, Z. Sljivancanin, M. Mavrikakis, J. Catal. 209 (2002) 275–278.